nature communications

Supplementary Materials for

Melt Densification Enables Fracture-resistant Blend Hydrogels

Xunan Hou[1], Zichun Zhu[1], Yuting Wen[2], Yixin Zhang[1,3], Chitinart Thedrattanawong[2], Daria V. Andreeva[1,3], Jun Li[2], Chaobin He[1,4]*
Corresponding author: msehc@nus.edu.sg

The PDF file includes:

Materials and Methods
Supplementary Text S1 – S3
Figs S1-S12
Tables S1 to S6
References

Materials and Methods

Materials

Polymethyl methacrylate (PMMA, M_w ~ 70kDa, PDI = 1.3) were supplied by Sumitomo Chemicals (Singapore). Polyethylene glycol (PEG, M_n = 10kDa and 35kDa, PDI ~ 1.2), polyvinyl formal (PVF, M_w ~ 70kDa), anhydrous tetrahydrofuran (THF, ≥ 99.9%), PMMA (M_w = 120k and 350k) were purchased from Sigma-Aldrich. Benzophenone (BP, 99%) and acetone (ACS, 99.5%) were purchased from Thermo Scientific Chemicals, USA. These compounds were used directly without further purification.

Preparation of melt-crosslinked networks (MCN)

PMMA pellets were dissolved in 5mL acetone under continuous stirring at 50°C until a clear solution is formed. PEG flakes were added followed by BP for dissolution. The total polymer mass was ~1.5g, solution concentration was maintained at 50% wt., and PMMA mass fraction in the blend ϕ was varied from 0-0.6. The molar ratio of BP to ethylene glycol units in PEG (C_i) varied from 10^{-4} to 10^{-2}. The solution was degassed by sonication for 5min at 40 °C, casted onto a glass petri dish at 50°C for ~3 hours, followed by vacuum treatment at 50 °C for 2 hours to completely remove the solvent. The dried blends were hot pressed between two PE films at 0.2MPa for 2min, released for 1min and pressed again for 2min. The blend film is then place in a clear, food-grade polyethylene bag (~6cm*4 cm) and carefully sealed to eliminate residual air. The heating temperature varied between 60-80°C depending on the PMMA fraction.

The homogenized melt blend films in PE bags were cured in a 2000-EC UV flood curing system (Dymax®, US) at a range of 320-390 nm and nominal intensity of ~105 mW/cm². The samples were cured at intervals of 1.5min and flipped around at each interval for more homogeneous curing. The chamber surface temperature was ~45°C, which prevents PEG crystallization at curing, but lower than the boiling point of solvent. Solution blend networks were prepared following the same method, except that the solution was not dried, but directly sealed in a PE bag (8cm*6cm) for UV curing.

Swelling and Solvent Etching

The swelling ratio and water content of the hydrogels was determined by assessing their dry and wet mass in various cycles. As-prepared MCN sample was weighed immediately and immersed in DI water for swelling until the mass equilibrates to obtain its wet mass m_{wet}. Excess surface water was carefully removed using Kimwipes. To verify the swelling, the swollen hydrogels were then dried in a vacuum oven at 60°C to obtain the dry mass. The wet weight m_w and dry weight m_{dry} were measured using a microbalance. Swelling ratio was defined as SR = m_{wet}/m_{dry}, and the equilibrium water content was calculated as EWC = (1-1/SR) × 100%. Selective solvent etching of m_0 ~ 1g dry sample was performed at 50°C using anhydrous THF, where the sample was taken out at regular intervals, rinsed with DI water and weighed to obtain its mass *m*. The samples were then rehydrated in pure water to produce the etched hydrogels.

Characterization of MCN gels

Scanning Electron Microscopy (SEM)

The morphology of swollen and etched hydrogels was examined using a field-emission scanning electron microscope (Zeiss Supra 40 FE-SEM) operated at a voltage of 5 kV, aperture size 30μm. The hydrogel samples were immersed into liquid nitrogen for 5min, freeze-dried overnight and sputter-coated with ~8nm thick of gold layer. The etched samples were repeatedly washed with water before freezing.

Mechanical and fatigue properties

To measure ultimate properties, uniaxial tensile test of hydrogels were conducted on a double-column universal tester (Instron 5569, USA) equipped with a 100 N load cell. Fully swollen hydrogels were cut into rectangular specimens at dimension of 60 mm × 10 mm × 0.60 mm, with an initial gauge length H of ~10 mm. Unnotched specimens were subjected to monotonic stretch until failure at a strain rate of 1 min^{-1}. The elastic energy function W(ε) was obtained by integrating the area under the stress-strain (σ-ε) curve. To evaluate the fracture toughness Γ, a sharp blade was used to introduce a notch at the sample edge, and the specimen was stretched to failure, measuring the maximum strain ε_m . The toughness was defined by $W(\varepsilon_m)$ H. The fractocohesive length L is given by the ratio between notched toughness Γ and work of fracture E_f.

To measure cyclic properties and flaw-sensitivity, fatigue tests were performed using the single-edge notch method on a rectangular sample 60× 20 × 0.6 mm in size. A ~5mm notch was cut on the center long edge of the sample, then a cyclic stretch of predefined stress was applied to the sample under saturated humid condition supplied by a household humidifier (>90% R.H.). Each stress corresponds to an energy release rate G_c. The frequency of cyclic stretch was 0.5Hz, and 5000 cycle were performed for each G_c value. The applied stress for each sample corresponds to an amplitude of energy release rate, G_c. ~200 cycles of preloads were performed to form a stable crack tip. Total crack advance c was measured by an optical microscope after an additional N = 5000 cycles and divided by the number of cycles N to get the average crack propagation per cycle dc/dN, assuming c linearly increases in N. The loading rate was 0.5 Hz for all samples Fatigue threshold Γ_0 was interpreted from the X-intercept of dc/dn-G_c curve.

Wide-angle X-ray diffraction (WAXD)

Crystallization characteristics of hydrogels are measured by a Bruker GADDS X-ray diffractometer (D8 Advance) instrument at 40mA, 40kV, with Cu Kα radiation (λ = 1.5418 Å). Scanning range was 2θ = 10 - 40° at a total exposure time of 2000s. The samples were freeze-dried before each measurement and mounted onto a plastic sample holder. Backgrounds subtraction and smoothing were done on the instrumental software. The final data were normalized by sample thickness.

Differential scanning calorimetry (DSC)

Thermal properties of melt-crosslinked networks were measured on a Perkinelmer DSC6000. The freeze-dried samples were cut into pieces of ~2mm in size by a surgical scalpel (Swann-

Morton, USA). ~ 7 mg of sample pellets were sealed into a robotic pan and undergo DSC scan: cooling to -30 °C, and heating to 140 °C for 2 cycles. Heating rate was 10°C/min. The glass transition temperature (T_g) was obtained from the inflection point of step change. The crystallinity X_c in the samples was obtained by

$$X_c = \frac{\Delta H_m}{w\Delta H_c} \quad \text{(Eq. 1)}$$

where ΔH_m and ΔH_{cc} are the enthalpies of melting, w is the weight fraction of PEG in the blend. Note that for all blends at ϕ = 0.50, no cold crystallization is detected. and ΔH_c= 196.8 J/g is taken as the crystallization enthalpy of pure PEG 35k. Results are shown in Table S3.

Rheological properties

The storage moduli G', loss moduli G" of dry blends and swollen hydrogels are measured on an MCR302 rotational rheometer (Anton Paar, Austria) and parallel plate setup. For melt and solution cured blends, the hot-pressed samples were fully dried in vacuum oven followed by at different C_i and was placed onto the bottom plate at multiple temperatures, most used at 140 ± 0.5°C. For G' and G", the normal force was set to ~1 N, and the angular frequency was varied from 0.1 – 200 rad/s.

Oxygen transmissibility and water permeance test

Oxygen permeability (Dk/t) of the gel membranes is measured using on-line mass spectrometry.(*1*) The measurements are conducted with a bench-top mass spectrometric residual gas analyser (Hiden Analytical, HPR-20 TMS) according to a modified protocol based on ISO 18369-4(*2*). All the tests were carried out at total feed flow rate of 250 mL min^{-1} and argon sweeping flow rate of 50 mL_n min^{-1} under controlled pressure of 1bar and temperature of 21°C. The ^{36}Ar isotope signal was used as internal standard for mass spectrometric analysis to determine the permeate composition of sweep stream. Concretely, a fully swollen hydrogel film (diameter d = 40 ± 2mm, hydrated thickness t = 100 ± 20 µm) were secured between two concentric rubbery O-rings (~37mm). Before each test, the membrane was purged with helium/water mixture for at least 3 hours for MS signal to reach a stable state and the background was recorded. The inlet gas was then switched to moisture saturated air or water vapor. After the switching, permeate concentrations grew as a function of time to reach steady state and the permeation rate were calculated after reaching steady state for a sufficient time. For water permeability, the background signal was measured in dry argon gas for 3hrs, and saturated water vapor was introduced into the chamber until a steady state was obtained.

Cell culture

Mesenchymal stem cells (MSCs) were cultured in alpha-Modified Eagle Medium (α-MEM) (Gibco) supplemented with 10% fetal bovine serum (FBS) and 1% penicillin-streptomycin. The cells were incubated at 37 °C in a 5% CO_2 humidified atmosphere.

Hydrogel films were sterilized by soaking in 3% penicillin-streptomycin for 24 h, followed by exposure to UV light for 30 minutes. The films were then placed individually into a 24-well plate for cell seeding. MSCs were seeded at a density of 5 x 10^4 cells/well with the prepared films. Cell attachment, spreading and morphology were observed in a microscope (Olympus, Model IX51)

at 24, 48 and 72 h post-seeding. At each time point, cells were gently washed three times with PBS to remove non-adherent cells before observation.

At 72 hours, cell proliferation was quantified using the CCK-8 assay (Dojindo). For the assay, 10 µL of CCK-8 reagent was added to each well, and the plate was incubated at 37°C for 2 hours. Absorbance was measured at 450 nm using a microplate reader. A standard curve was generated by plotting absorbance values against known cell numbers. (Fig. S10) Using this cell number standard curve, the number of cells on each film was calculated based on the absorbance measured in the CCK-8 assay, allowing for an accurate estimation of cell proliferation on each film. Additionally, cell viability was assessed using a Live/Dead Cell Viability Assay. After 72 hours, the cells were washed with PBS and stained with 2 µM Calcein AM (for live cells) and 4 µM Ethidium Homodimer-1 (for dead cells) for 30 minutes at 37°C. A fluorescence microscope (Olympus, Model IX71) was used to observe live (green) and dead (red) cells.

Assay for protein adsorption measurements

Protein adsorption was evaluated using an artificial tear solution of PBS containing bovine serum albumin (BSA, Sigma Aldrich). In a typical procedure, as-prepared hydrogels were punched on a film cutter to make standard sized gel films(d = 16mm, t = 100 ± 20µm). The films were then washed and equilibrated in pure PBS for 24 hours and incubated in BSA solution (1 mg/mL) at pH 7.4 for 72 hours. After rinsing with PBS for 3 cycles to remove loosely bound albumin, the absorbed proteins were recovered by 200µL 1% sodium dodecyl sulfate (SDS). The quantity of absorbed protein was determined using a Pierce™ BCA Protein Assay Kit and calculated after background correction for each protein solution. (Fig. S12)

Molecular dynamics (MD) simulations

Molecular dynamics (MD) simulations are conducted using the Blends Module in Materials Studio® software. This module incorporates temperature dependence into the interaction parameter, achieved by generating a substantial ensemble of pair configurations and calculating their binding energies. The results are then averaged over temperature using the Boltzmann factor to derive the temperature-dependent interaction parameter.

Supplementary Text

S1. Theory for polymer modeling

Unlike the original Flory-Huggins theory, which assumes a regular lattice arrangement, Blends employs an off-lattice approach, allowing for a more realistic representation of molecular configurations. Chemical simulations are utilized to accurately determine the coordination number for each potential molecular pair. By incorporating a temperature-dependent interaction parameter $\chi_M(T)$ into the Flory-Huggins equation, the free energy can be evaluated across various compositions and temperatures. Additionally, factors such as packing variables and chain connectivity are considered, with specific atoms marked to exclude them from contact interactions. The excluded-volume constraint technique is employed to calculate the binding energy between molecules of components i and j. This binding energy quantifies the interaction

strength between the two components, and in conjunction with the coordination numbers, facilitates the calculation of mixing energy and the χ_M parameter.

Theories concerning phase behavior of polymer blends include Flory Huggins (FH) theory(3) and self-consistent field theory (SCFT).(4, 5) The most widely applied classical FH model arranges monomeric units into lattices.(3, 6) The model provides a general expression for binary mixtures that accounts for various thermodynamic contributions.

The thermodynamic and phase behavior of polymer mixtures under different conditions are described by several theories, including lattice theory and self-consistent field theory specifically for microphase-separated systems. Among these, the Flory-Huggins model is the most widely utilized, as it simplifies the complexities of polymer mixing into a lattice framework. The model provides a general expression for binary mixtures that accounts for various thermodynamic contributions.

$$\frac{\Delta G_m}{RT} = T\Delta S_m + \Delta H_m = (\frac{\Phi_1}{n_1} ln\Phi_b + \frac{\Phi_2}{n_2} ln\Phi_1) + \chi_M \Phi_1 \Phi_2 \qquad \text{(Eq. S1)}$$

where R is the gas constant, T is temperature in kelvin, Φ_i and n_i are the molar fractions and number of repeat units in component i (i = 1,2), respectively. The SCFT theory and its later extensions concerns the interfaces of immiscible blends/ block copolymers by scattering methods such as SAXS.(4) These techniques are more suited to two phase systems, such as amorphous polymer blends or block copolymers, but faces difficulties in semicrystalline blends due to scattering from crystals. According to SCFT, the interfacial thickness a_I scales inversely with $\chi^{1/2}$. Thus, weakly interacting blends often show wider (diffused) interfaces than strongly interacting blends. SAXS results of our previous contribution have supported this point.

The critical condition for miscibility is formally defined by the spinodal condition

$$\left(\frac{\partial^2 \Delta G_m}{\partial \phi_i^2}\right)_{T,p} = 0 \qquad \text{(Eq. S2)}$$

leading to a critical interaction parameter

$$\chi_c' = \frac{1}{2}\left(\frac{1}{\sqrt{n_1}} + \frac{1}{\sqrt{n_2}}\right)^2 \qquad \text{(Eq. S3)}$$

which indicates the onset of phase separation. The original Flory-Huggins theory, however, does not consider several important factors such as temperature dependence and lattice irregularities.(6–8) By employing structural and spectral data to define parameters, accurate force fields could be generated to facilitate MD simulations. This work applies such an force field to account for temperature fluctuation within the system.

S2. Chain network properties and mechanics of MCN gels

Assuming full utilization of initiator radicals during photoreaction, the number of crosslinks per chain can be deduced by

$$N_c = \frac{M_{PEG} \cdot C_i}{M_{EG}} \qquad \text{(Eq. S4)}$$

while the segmental length between crosslinks:

$$L_c = \frac{M_{PEG}}{N_c+1} \quad \text{(Eq. S5)}$$

Different from conventional single and double networks where one or both networks are fully cured (albeit with defects), the blend network features physical entanglements and chemical crosslinks, which makes its rheological characterization a non-trivial task. Nonetheless, effects of co-existing crosslinks and entanglements can be decoupled qualitatively by its crossover modulus G_x and plateau modulus G_N^0. The G_N^0 characterizes the entanglement and crosslink density in molten polymer blends and elastomers from the crossover modulus G_x, defined by the intersection of G' and G" in oscillatory frequency sweep. The characteristic relaxation time τ_R corresponding to solid–liquid like transition is deduced from $\tau_R = \frac{1}{2\pi\omega_x}$

where ω_x is the crossover frequency at G_x (G' = G'').

S3. Molecular weight (M_w) effects

The M_w of polymers affects network formation and mechanical properties (Table S1). The critical molecular weight M_c, usually 2-3 times of entanglement molecular weight M_e, is a key parameter for chain network formation. When neat PEG is crosslinked at a lower molecular weight of 2000, the stiffness can be increased to ~ 700kPa, but elongation drops to ~50%. The M_w effects are verified experimentally, and results are shown in Table S1. When substituting PMMA with its short-chain counterpart (M_w = 15 kDa ~M_e), MCN network could not form due to insufficient entanglements, and the gels disintegrate in water within 2 hrs. Reducing PEG chain length (M_w =10k) leads to stiffer chains and lower elongation at breaks (~150%). On the other hand, increasing PMMA M_w (120kDa and 350kDa) does not significantly alter mechanical properties, suggesting that the entanglement limit is set by PEG network rather than PMMA.

Table S1.

Physical properties of blend hydrogels by processing, composition and M_w.

Sample[1]	SR (g/g)	E (MPa)[2]	σ (MPa)[2]	ε (%)[2]
PEG/PMMA solution	2.15±0.06	54.68±1.23	1.95±0.12	45.62±3.35
PEG/PMMA melt	2.18±0.05	37.25±0.95	3.36±0.16	231.08±12.84
PEG/PMMA ϕ=0.33	3.01±0.08	7.53±0.45	1.25±0.08	209±15.42
PEG/PVF melt	4.01±0.12	1.27±0.18	0.115±0.02	70.19±5.38
PEG10k/PMMA	1.98±0.05	49.25±0.22	2.95±0.21	151±13.58
PEG/PMMA120k	2.05±0.03	36.75±0.86	3.52±0.19	252.13±20.58
PEG/PMMA350k	2.11±0.05	33.45±0.75	3.68±0.14	228.95±18.73

[1]Unless otherwise stated, PMMA M_w = 70k and ϕ=0.50, C_i=0.005; [2]tested at equilibrium swollen state.

Table S2.

Solubility parameters of polymers used in this work

	δ_d	δ_p	δ_v	δ_h	δ
PEG	16.3	10.2	19.2	8.7	21.1
PMMA	17.0	5.8	18.0	9.1	20.2
PVF	16.7	4.9	17.4	8.6	19.4

Table S3

Thermal properties of neat polymers and crosslinked blends (ϕ = 0.50)

	T_g (°C)	$T_{m,PEG}$ (°C) [1]	H_m (J/g) [1]	X_c (%)
PVF	107.8	-	-	
PMMA	103.5	-	-	
PEG	-59[2]	64.5	166.08 ± 3.76	84.39
PEG/PVF	106.5[1]	63.6	63.46 ± 2.95	64.43
PEG/PMMA	ND[3]	48.5	48.26 ± 2.18	48.98

[1]Data acquired at heating rate of 10°C/min. [2] from literature [3]ND: not detected.

Table S4

Range of mechanical properties in melt-crosslinked gels with other tough gels and biological tissues

Material	Modulus (MPa)	Toughness (kJ/m^2)	Fatigue threshold (J/m^2)	Reference
Conventional gels	0.01-0.09	0.01-0.05	1.8-6.8	(*9*)
Entangled SN gel	0.15-0.4	0.05-0.8	45-130	(*10*, *11*)
DN gel	0.09-1.5	0.08-0.6	90-300	(*12*, *13*)
Annealed PVA gel	1.0-1.8	0.6-2	350-850	(*14*)
Dehydrated gel	0.1-0.15	5-10	297	(*15*)
Contact lens	0.03-0.2	0.07-0.35	75-347	(*16*)
Cartilage	2.1-8.9	0.14-1.2	0.14-1.46	(*17*)
Elastomers	20-250	1.5-3.6	15-90	(*10*)
MCN gel	0.3-35	0.7-24.5	1100-3400	This work

Table S5.

Summary of mechanical properties in MCN gels

PMMA	E_f	Γ	Γ_c	L
%	MJ/m^3	J/m^2	J/m^2	mm
0	1.1	20	8	0.20
20	8.3	702	1074	0.87
25	18.8	2230	1378	1.19
33	36.0	5840	1837	2.03
50	105	19800	3100	2.36
60	150	24500	3404	2.18
100	0.9	1200	0.1	0.57

Table S6.

Protein absorption of some common contact lens materials

Material	BSA absorbed (μg cm^{-2})	Reference
HEMA	3.95 ± 0.20	(*18*)
HEMA-MMA	0.98 ± 0.02	(*19*)
HEMA-HACC	1.45 ± 0.05	(*18*)
Neat PEG	21.34 ± 1.27	(*20*)
PEG-pCBAA	11.01 ±0.88, 9.90 ± 0.89, 8.94 ± 0.48	(*20*)
PEG-PSU	8.0 ± 1.55	(*21*)
PDMS	3.09 ± 0.26	(*22*)
PDMS-MPC	0.55 ± 0.11	(*22*)
MCN gels	0.38-0.55	This work

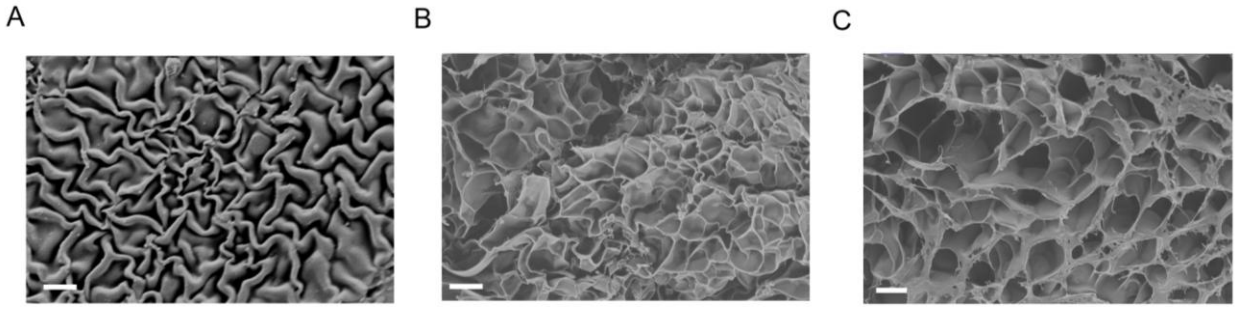

Fig. S1.

SEM images of MCN gels (ϕ = 0.5) etched for different durations: (A) 1min; (B) 5min; (C) 30min.

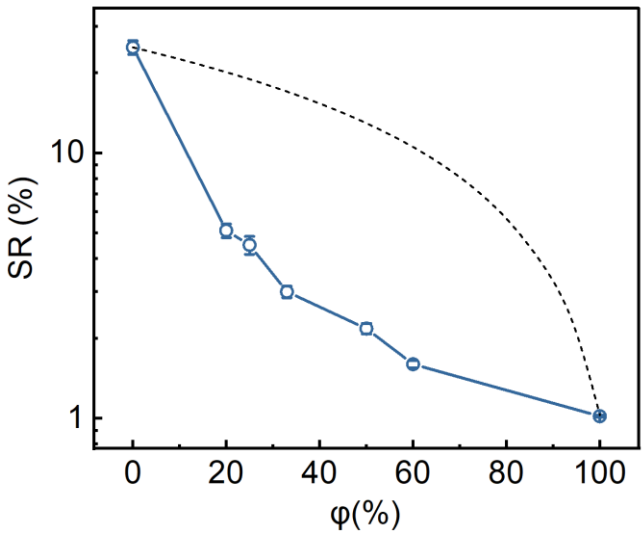

Fig. S2.

Swelling ratio (SR) of PEG/PMMA hydrogels. Dashed line denotes mixture rule prediction.

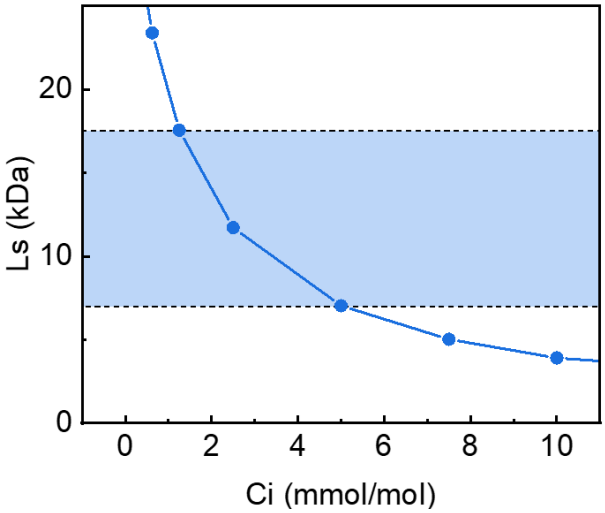

Fig. S3.

Chain length between crosslinks L_s as a function of initiator concentration C_i. blue zone indicates entanglement dominant range, higher L_s does not form hydrogels, while lower L_s results in stiff gels.

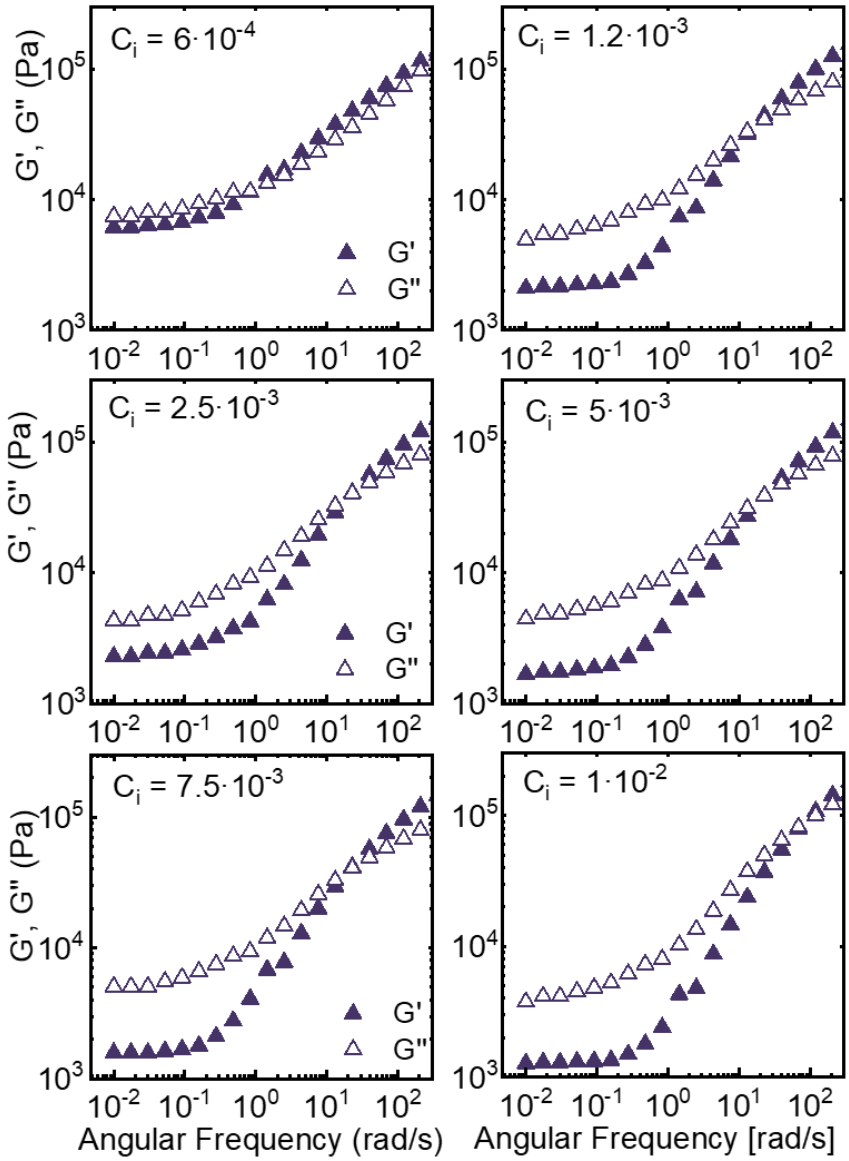

Fig. S4.

Storage and loss moduli of MCN. C_i values from $6 \cdot 10^{-4}$ to $1 \cdot 10^{-2}$. All data were obtained in frequency sweep at 140 °C

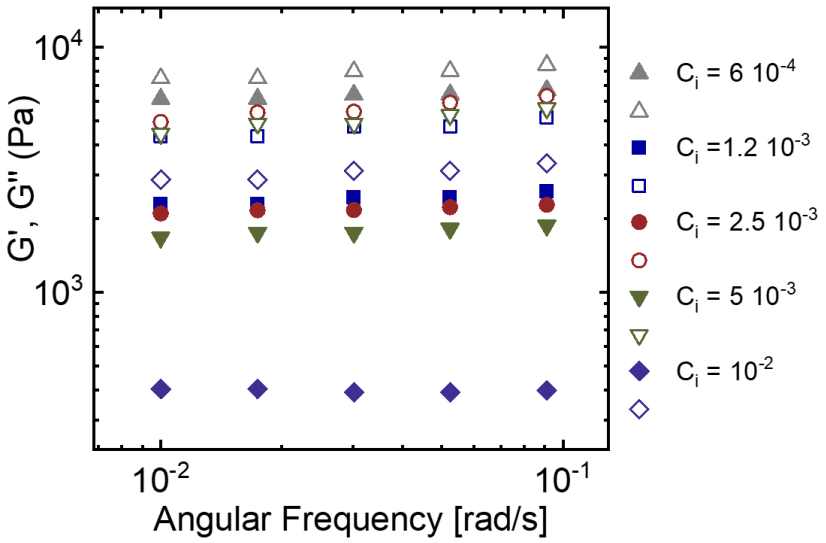

Fig. S5.

Storage and loss moduli of MCN at low frequencies.

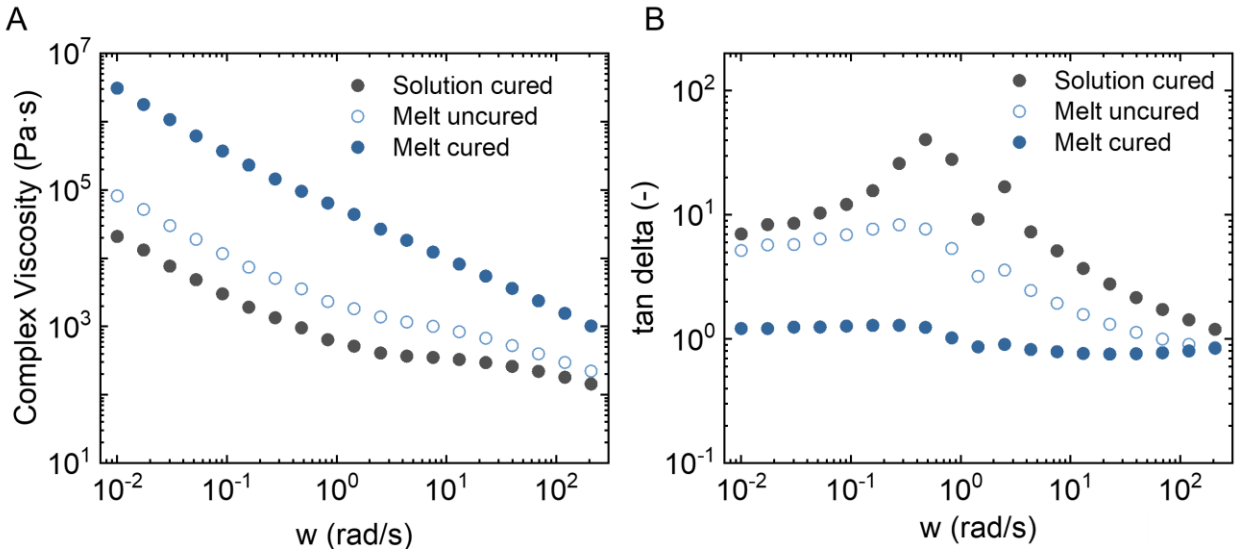

Fig. S6.

Rheological properties of solution and melt cured samples. (A) Complex viscosity η; (B) loss tangent tanδ. Maximum dissipation occurs at medium frequency which corresponds to a transition from highly viscous to more elastic state at faster shear. All data were acquired in frequency sweep at 140°C.

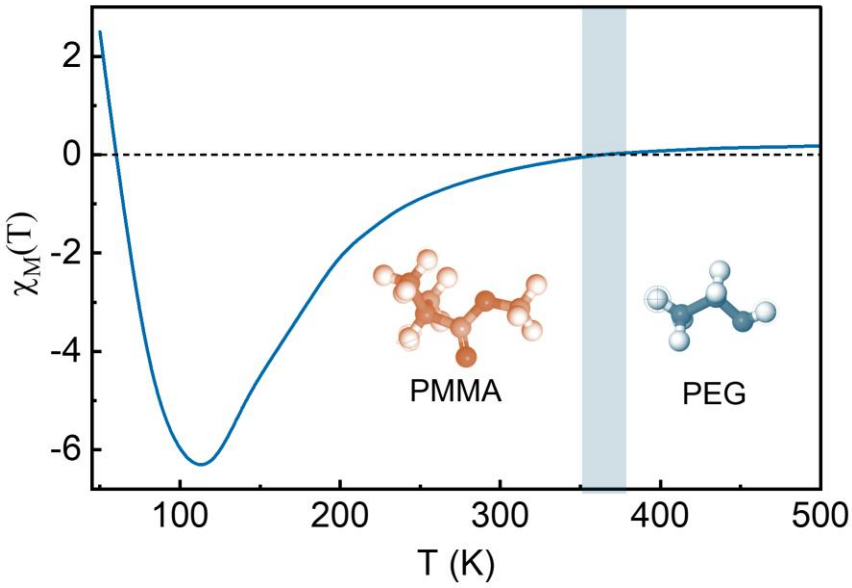

Fig. S7.

Interaction parameter χ as a function of temperature T for PEG/PMMA blend. Inset: Schematics of repeat units in both polymers. The blue zone depicts the optimal blending temperature range.

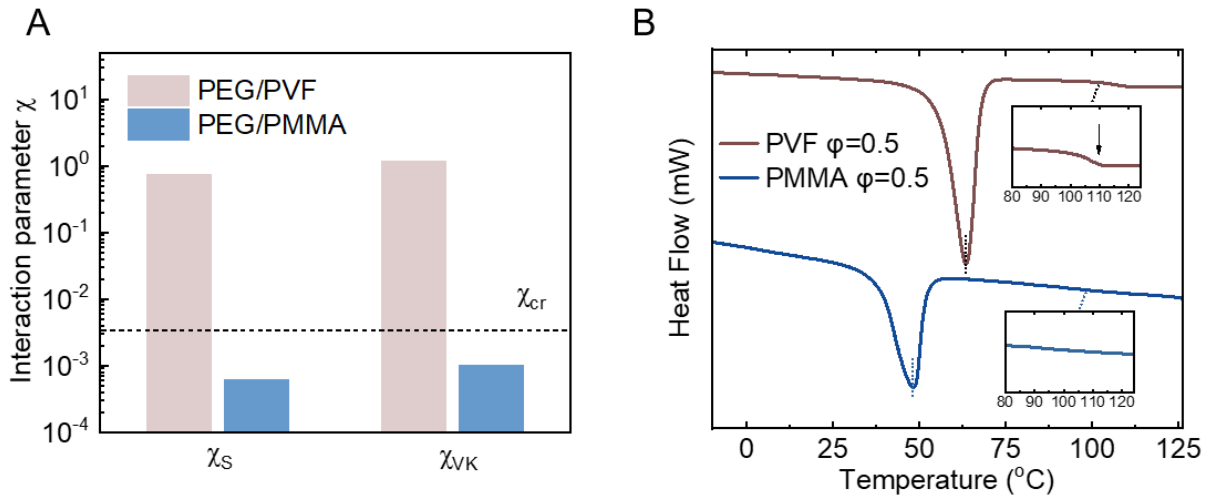

Fig. S8.

Comparison of miscible and immiscible blend gels: (A) Interaction parameter estimated by two methods χ_s and χ_{VK}; dotted line indicates critical value χ_{cr}. (B) Differential scanning calorimetry curves

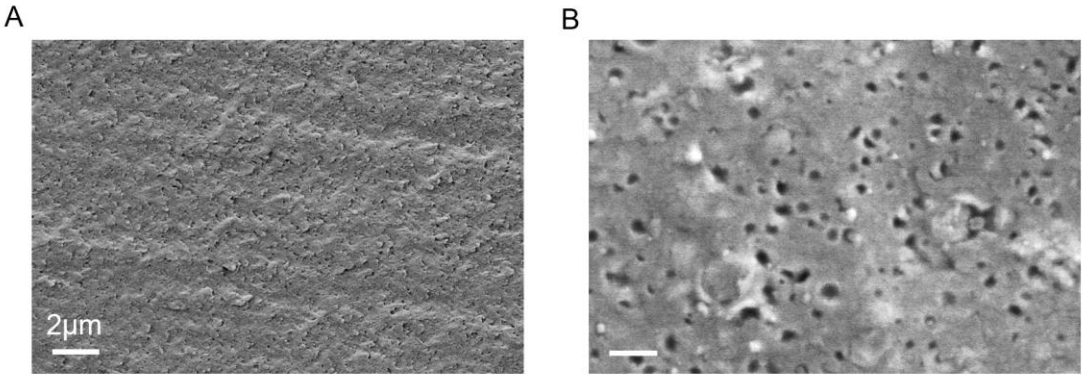

Fig. S9.

SEM images of cryo fractured freeze-dried surfaces: (A) PEG/PMMA; (B) PEG/PVF. Φ = 0.33 in both samples. Scales are 2 µm.

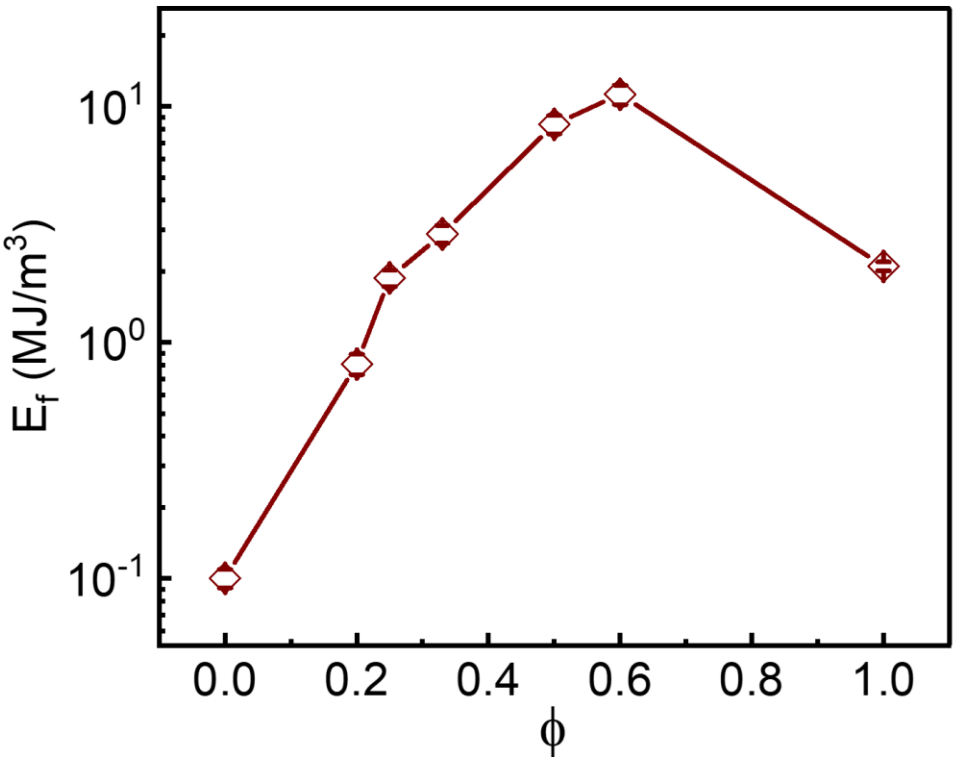

Fig. S10.

Work of fracture E_f in MCN blends as a function of PMMA fraction ϕ.

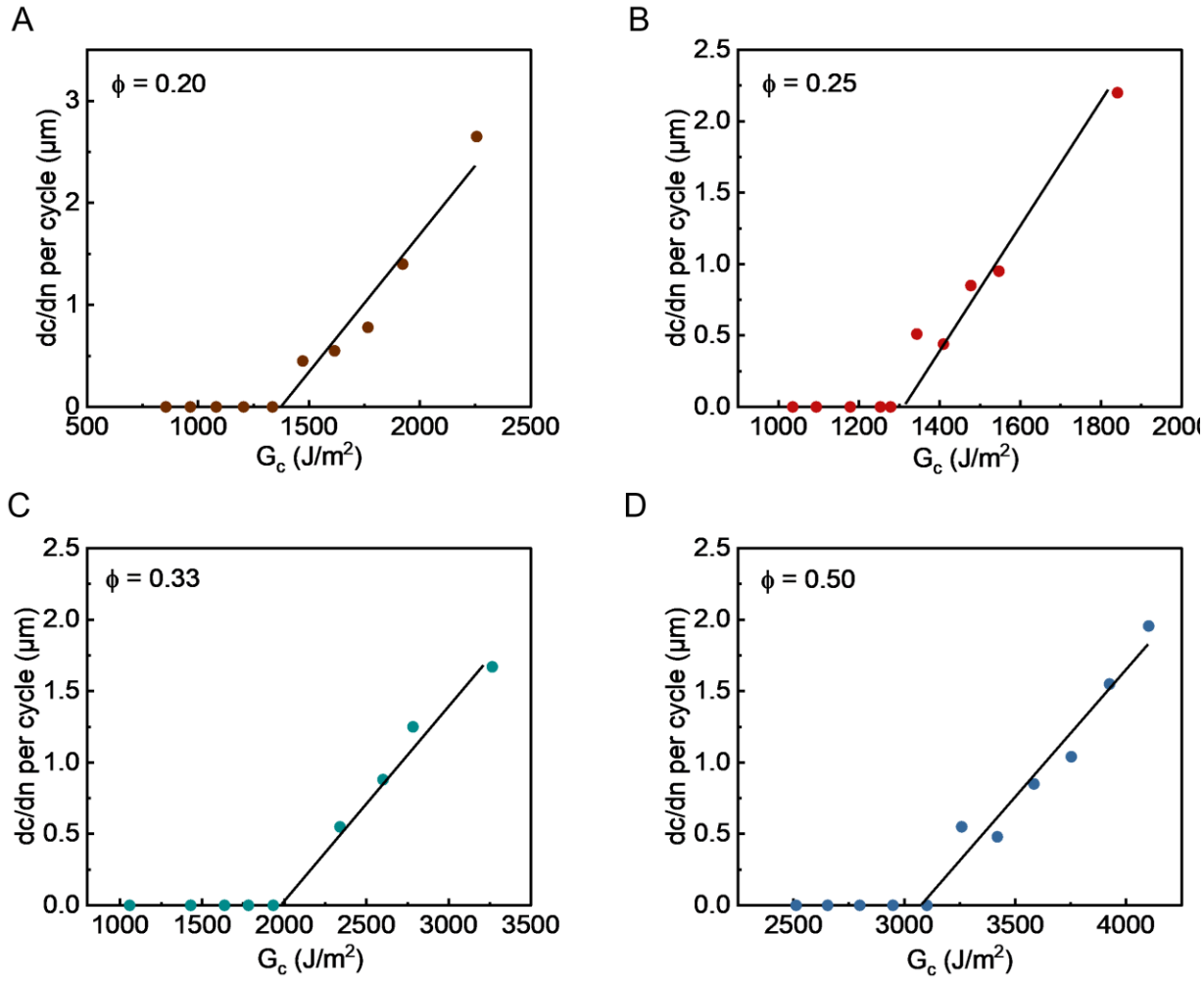

Fig. S11.

Crack propagation per cycle dc/dn versus energy release rate G_c at various ϕ values

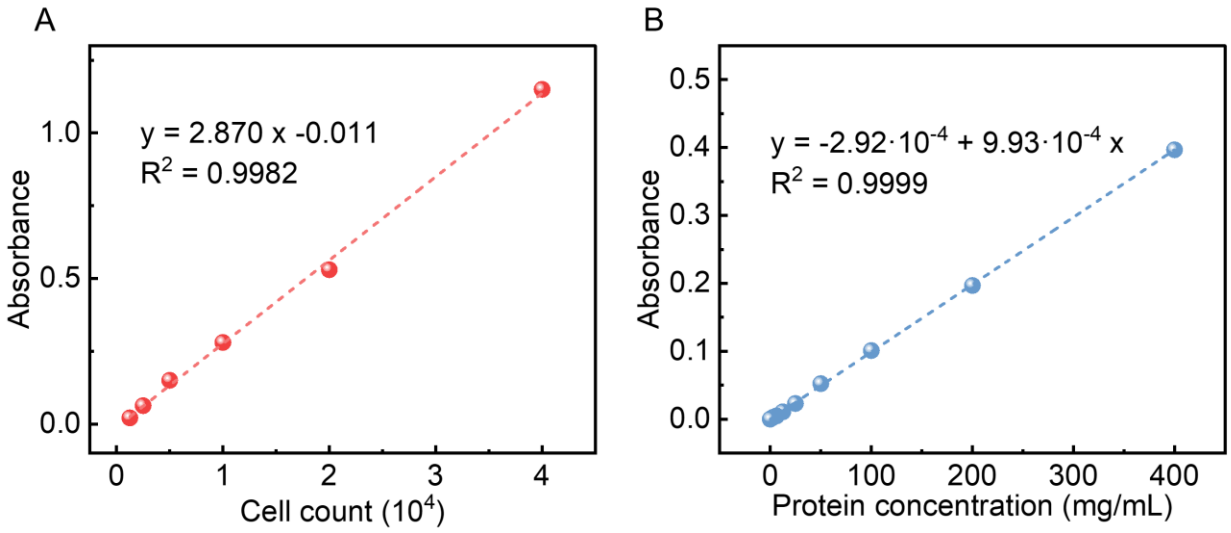

Fig. S12.

Standard curve for (A) Cell counts versus absorbance; (B) Protein concentration in BSA assay

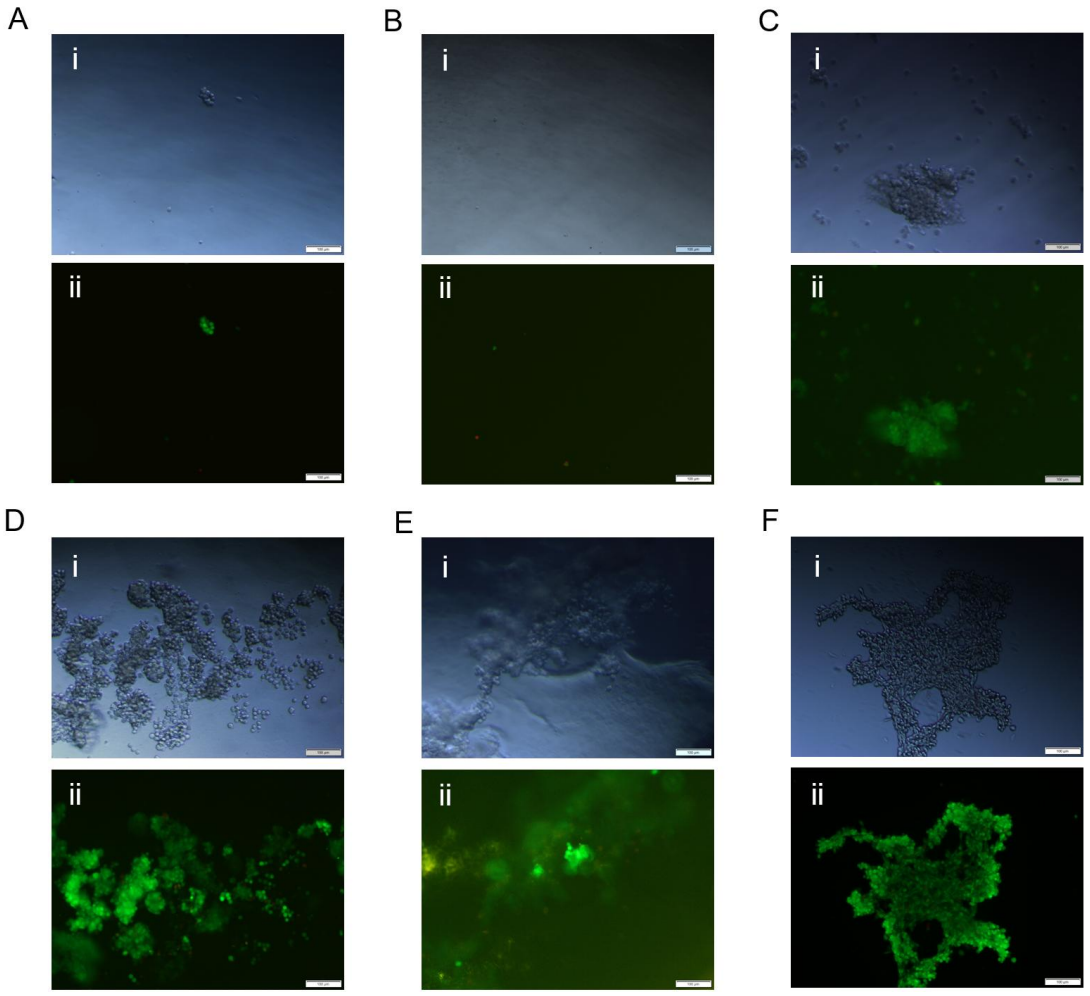

Fig. S13.

(i) Bright field and (ii) Fluorescence images of cells on MCN gels of different ϕ values at day 3: (A) 0.50; (B) 0.33 (C) 0.25 (D) 0.20 (E) 0.16 (F) Control substrate. Scales are 100 µm.

SI references

1. M. Chen, M. Trubyanov, P. Zhang, Q. Wang, Z. Li, K. S. Novoselov, D. V. Andreeva, Comprehensive characterization of gas diffusion through graphene oxide membranes. *J Memb Sci* **676**, 121583 (2023).
2. BS EN ISO 18369-4:2017: Ophthalmic optics. Contact lenses: Physicochemical properties of contact lens materials . British Standards Institute [Preprint] (2018). https://go.exlibris.link/RStG3C4H.
3. P. J. Flory, Thermodynamics of high polymer solutions. *J Chem Phys* **10**, 51–61 (1942).
4. E. Helfand, Block copolymers, polymer-polymer interfaces, and the theory of inhomogeneous polymers. *Acc Chem Res* **8**, 295–299 (1975).

5. D. Brosetav, G. H. Fredrickson, E. Helfand, L. Leibler, Molecular Weight and Polydispersity Effects at Polymer-Polymer Interfaces. *Macromolecules*, doi: 10.1021/ma00203a023 (1990).
6. H. B. Eitouni, N. P. Balsara, "Thermodynamics of Polymer Blends" in *Physical Properties of Polymers Handbook* (Springer New York, New York, NY, 2007), pp. 339–356.
7. E. Meaurio, N. Hernandez-Montero, E. Zuza, J.-R. Sarasua, "Miscible Blends Based on Biodegradable Polymers" in *Characterization of Polymer Blends* (Wiley-VCH Verlag GmbH & Co. KGaA, Weinheim, Germany, 2014), pp. 7–92.
8. R. H. Colby, M. Rubinstein, Polymer physics. *New-York: Oxford University* **100**, 274 (2003).
9. X. Hou, B. Huang, L. Zhou, S. Liu, J. Kong, C. He, An Amphiphilic Entangled Network Design Toward Ultratough Hydrogels. *Advanced Materials* **35** (2023).
10. J. Kim, G. Zhang, M. Shi, Z. Suo, Fracture, fatigue, and friction of polymers in which entanglements greatly outnumber cross-links. *Science* **374**, 212–216 (2021).
11. G. Nian, J. Kim, X. Bao, Z. Suo, Making Highly Elastic and Tough Hydrogels from Doughs. *Advanced Materials* **34**, 2206577 (2022).
12. W. Zhang, X. Liu, J. Wang, J. Tang, J. Hu, T. Lu, Z. Suo, Fatigue of double-network hydrogels. *Eng Fract Mech* **187**, 74–93 (2018).
13. C. Imaoka, T. Nakajima, T. Indei, M. Iwata, W. Hong, A. Marcellan, J. P. Gong, Inverse mechanical-swelling coupling of a highly deformed double-network gel. *Sci Adv* **9** (2023).
14. S. Lin, X. Liu, J. Liu, H. Yuk, H.-C. Loh, G. A. Parada, C. Settens, J. Song, A. Masic, G. H. McKinley, X. Zhao, Anti-fatigue-fracture hydrogels. *Sci Adv* **5**, 1–9 (2019).
15. D. Zhong, Z. Wang, J. Xu, J. Liu, R. Xiao, S. Qu, W. Yang, A strategy for tough and fatigue-resistant hydrogels via loose cross-linking and dense dehydration-induced entanglements. *Nat Commun* **15** (2024).
16. A. P. Jackson, Measurement of the fracture toughness of some contact lens hydrogels. *Biomaterials* **11**, 403–407 (1990).
17. D. Taylor, N. O'Mara, E. Ryan, M. Takaza, C. Simms, The fracture toughness of soft tissues. *J Mech Behav Biomed Mater* **6**, 139–147 (2012).
18. X. Lin, J. Liu, F. Zhou, Y. Ou, J. Rong, J. Zhao, Poly(2-hydroxyethyl methacrylate-co-quaternary ammonium salt chitosan) hydrogel: A potential contact lens material with tear protein deposition resistance and antimicrobial activity. *Biomaterials Advances* **136**, 212787 (2022).
19. W. Zhang, G. Li, Y. Lin, L. Wang, S. Wu, Preparation and characterization of protein-resistant hydrogels for soft contact lens applications via radical copolymerization involving a zwitterionic sulfobetaine comonomer. *J Biomater Sci Polym Ed* **28**, 1935–1949 (2017).
20. T. Wang, J. Deng, R. Ran, W. Shi, Y. Gao, X. Ren, J. Cao, M. Zhang, In-situ forming PEG-engineering hydrogels with anti-fouling characteristics as an artificial vitreous body. *Chemical Engineering Journal* **449** (2022).
21. D. Zhong, Z. Wang, J. Zhou, Y. Wang, Additive-free preparation of hemodialysis membranes from block copolymers of polysulfone and polyethylene glycol. *J Memb Sci* **618** (2021).

22. F. Sun, X. Li, J. Xu, P. Cao, L. Xiao, Improving hydrophilicity and protein resistance of silicone hydrogel by plasma induced graft polymerization of 2-methacryloyloxyethyl phosphorylcholine. *E-Polymers*, 1–11 (2011).